ISRAEL JOURNAL OF TECHNOLOGY, Vol. 11, No. 4, 1973, pp. 253–265
Proc. Seventh Isr. Conf. MECHANICAL ENGINEERING, June 1973

The Prediction of The Performance of Variable Geometry Free Gas Turbines

D. ADLER*

Department of Mechanical Engineering,
Technion—Israel Institute of Technology, Haifa, Israel

M. HIRSCH**

Beit Shemesh Engines, Beit Shemesh, Israel

and

Y. DAYAN*

Department of Mechanical Engineering,
Technion — Israel Institute of Technology, Haifa, Israel

ABSTRACT

The prediction of the performance of gas turbines for known geometry is based on the equations of flow subject to loss calculations. All known prediction methods use experimental information for their calculations. Here a method is presented which utilizes experimental data selected from available sources to best fit the conditions in variable geometry gas turbines. The article gives a survey of the presently known loss calculation methods, discusses the combination of differently-defined loss coefficients and describes the prediction method.

NOTATION

A — flow cross section
B — a quantity used for convergence in the iterative calculation
b — length of profile center line
C — chord length
c — sound velocity
c_p — specific heat
D — a quantity used for convergence in the iterative procedure
e — radius of curvature of the profile backside
G — flow rate
g — gravitational acceleration
h — enthalpy
h_p — height of the blade
i — incidence angle
J — units transformation coefficient
K_p — specific heats ratio
k — blade tip clearance
M — torque
Ma — Mach number
N — speed of revolution of the rotor
N_{PT} — profile loss correction factor
N_{Pi} — incident loss correction factor
N_{PR} — Reynolds effect correction factor
O — blade passage opening
P — pressure
Q — normalized flow rate $\left(Q = \frac{G\sqrt{T_{1t}}}{P_{1t}}\right)$
R — gas constant
Re — Reynolds number
s — blade pitch
T — temperature
t_e — trailing edge thickness
u — peripheral velocity

* Senior Lecturer
** Engineer

V — absolute velocity
W — relative velocity
X — energy loss coefficient
Y — total pressure loss coefficient
α — absolute angle
α^0 — design angle
β — relative velocity angle
Δx — additional loss
$\Delta\alpha$ — flow deflecion angle at stator exit
$\Delta\beta$ — flow deflection angle at rotor exit
θ — angular position of stator vanes
μ — dynamic viscosity
η — efficiency
ρ — density

Subscripts

1 — stage inlet
2 — stator exit and rotor inlet
3 — rotor exit
a — annulus
B — blade
c — tip clearance
i — incidence angle or initial iteration value
l — final iteration value
M — Mach number
P — profile
R — Reynolds number
rel — relative
rot — rotor
s — isentropic
sc — secondary
st — stator
s/e — back side curvature of the profile
T — blade geometry
t — total

1. INTRODUCTION

This work describes a mathematical model for the prediction of the performance of a gas turbine stage (not to be confused with a complete gas turbine) equipped with a variable geometry nozzle. The model was developed to determine the influence of the basic turbine parameters such as blade and turbine geometry, thermodynamic inlet conditions, nozzle guide vanes angle, and speed, on the flow in the stage components and on the characteristics of the turbine stage. This information is required as a basis for a comprehensive mode ldescribing two shaft gas turbines with variable nozzle geometry and for the design of their dynamic control system (*Hirsch et al.*, to be published). In the stage model the nozzle and rotor are considered to be macroscopic control volumes used to describe the thermodynamic properties at the exit of each of these stage elements. The flow in the stage is considered to be one-dimensional, no information on two-or three-dimensional flow field properties is determined. Instead an appropriate blend of published relevant experimental information on the real flow and the losses in the stage components is incorporated in the model and superimposed on the simple one-dimensional formulation.

The model is solved numerically using a computer (IBM 370/165). Thus some aspects of the numerical procedure are discussed. The calculation can not be carried out in a straightforward fashion and an iterative procedure is required, so that special care must be given to convergence problems. Because of the shape of the stage characteristic (pressure vs. flow rate curve) two convergence criterions are required. Further the possibility of choking in the nozzle or in the rotor or in both, complicates the convergence procedure. All these are discussed below.

Figures 1 and 2 define the basic geometry and the thermodynamic quantities of the turbine stage. It must be pointed out here that the nozzle blade angles α_1 and α_2 are variables in the present model. The angle difference $\theta = \alpha_1 - \alpha_1^0$ (where α_1 is the instantaneous value and α_1^0 is the design point value) is one of the basic parameters studied in the present work.

2. CALCULATION OF THE LOSSES AND REAL FLOW EFFECTS

In the present study a mathematical model of a turbine stage is developed in which predicted stage losses are superimposed on the well known simple one-dimensional turbo machine theory. This approach cannot be avoided if work is to be kept within reasonable bounds. Thus the dominant part of the stage model is the calculation of the losses which actually represent the real three-dimensional flow field effects not

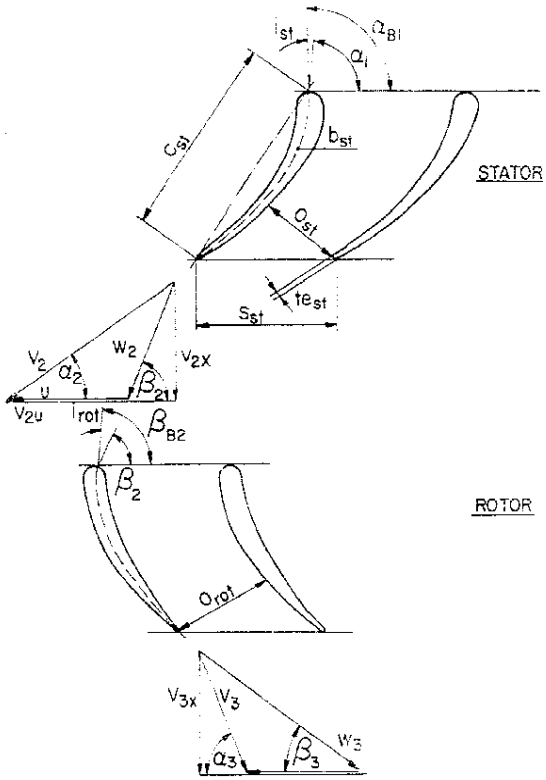

Fig. 1. The stage blading and the velocity diagrams.

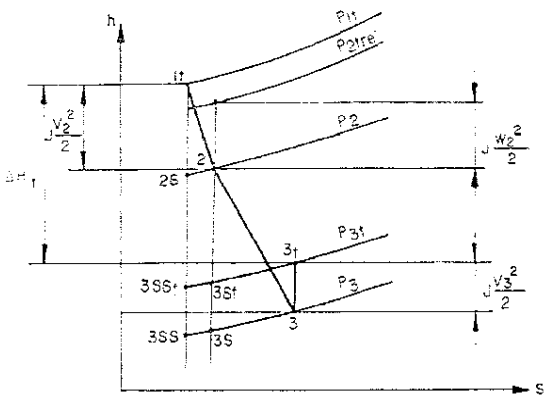

Fig. 2. h, s diagram of the expansion in the turbine.

included in the one-dimensional flow model. The sensitivity of the mathematical model to variations of the stage geometry depends strongly on the accuracy of the loss modeling. As many relevant stage parameters as possible must be included in the model to represent the real situation. Most known turbine stage loss prediction methods are based on the same basic turbine parameters (*Ainley and Mathieson*, 1957; *Dunham and Came*, 1970; *Horlock*, 1966; *Craig and Cox*, 1971; *Rahnke*, 1969) and on a similar approach to the loss calculation. A total loss coefficient is defined as a basic loss factor (depending on the cascade geometry) which is corrected using a number of coefficients depending on the character of the flow through the cascade. The loss factor can be defined in terms of energy losses

$$X = 100\frac{h_2 - h_{2s}}{JV_2^2/2} \tag{1}$$

or in terms of total pressure loss

$$Y = \frac{P_{1t} - P_{2t}}{P_{2t} - P_2} \tag{2}$$

these two loss factors are related as follows (*Hawthorne*, 1964):

$$X = 100\left(\frac{T_{2s}}{T_{1t}}\right)Y \tag{3}$$

The total loss factors are described by the following functional relation

$$X \text{ or } Y = f\left(Re, Ma, i, \text{blade geometry}, \frac{s}{b}, \frac{C}{h_e}, \frac{i_e}{s}, \frac{s}{e}, \frac{O}{c}, \frac{k}{h_e}\right). \tag{4}$$

This total loss factor is composed of the following partial loss coefficients

a) X_p or Y_p: profile loss

b) X_e or Y_e: annulus loss

c) X_{sc} or Y_{sc}: secondary loss

d) X_c or Y_c: blade tip clearance loss

In the present study a number of loss coefficient prediction methods are combined to form an optimal description of a turbine stage with a variable geometry nozzle. Profile losses are calculated using Craig's method (1971). The advantage of this method is that the effects of incidence conditions on the profile losses are well represented over a wide range of angles eliminating the necessity for extrapolation. This is extremely important in the case of adjustable nozzle blade stages, and when off design operation of stage is to be predicted.

The secondary losses representing three dimensional flow field effects in the cascades and in the stage flow

passages are calculated with Ainley's method (1957) modified and improved by Dunham (1970). This method is prefered for gas turbine modeling as also suggested by Horlock (1966) and Rahnke (1969). Craig defines his loss coefficient on the basis of energy, (Eq. 1) while Ainley uses total pressure loss coefficients, (Eq. 2). In the present work energy loss coefficients are preferred and Eq. 3 is used to transform Ainley's factors.

The losses calculated are incorporated in the turbine model and determined as the calculation proceeds. This is described in the next section.

3. THE MATHEMATICAL MODEL OF THE TURBINE

The model consists of a system of simultaneous equations which satisfy continuity, energy conservation, momentum (force equilibrium) and the equation of state. In addition the model includes experimental information and correlations for the losses. The equations are given below, but the sequence in which they are used in the solution as controlled by the computer program is given in Fig. 3 where the equations used in each computation step are given by the numbers in brackets. Because a complicated iterative procedure is required for the solution the sequence in which the equations are incorporated into the model is not unique and depends on the conditions at the point of operation for which the calculation is carried out. These conditions and their effect are best understood from Fig. 4, where three regions are defined: region 1 where the flow rate is an increasing function of the pressure ratio over the turbine stage, this is the low subsonic flow region; region 2 where the flow rate is a decreasing function of the pressure ratio, this is the high subsonic flow region; and region 3 where flow is choked and sonic flow is reached at a point in the turbine stage. In each region a different independent iteration variable is applied. When the point of operation is located in region 1, Q, the normalised mass flow rate parameter $(G\sqrt{T_{1t}}/P_{1t})$, is the most efficient independent iteration variable. When the point of operation is located in region 2, the pressure ratio is chosen to be the independent variable othe wise instabilities in the solution can not be avoided because P_{3t}/P_{1t} is a double valued function of Q in this region. In region 3, Q is constant so that iteration conditions are entirely different but this region is not dealt with in the present paper. As the independent iteration variable is not unique, the iterative procedure and thus sequence in which the equations are incorporated into the mathematical model depend on the regions in which the points of operation of the nozzle and of the rotor are located during the calculation.

The equations to be incorporated in the mathematical model as chosen by the computer program are grouped into two groups:

I) Equations relevant to the nozzle

Energy equations

$$J\frac{V_2^2}{2} = -\int_{T_{1t}}^{T_2} c_p(T)dT \tag{5}$$

$$J\frac{V_{2s}^2}{2} = -\int_{T_{1t}}^{T_{2s}} c_p(T)dT \tag{6}$$

Continuity

$$G = \frac{P_2 A_2 V_2}{R T_2} \tag{7}$$

Equation of state in isentropic flow

$$JRg\ln\frac{P_2}{P_{1t}} = \int_{T_{1t}}^{T_{2s}} \frac{c_p(T)}{T}dT \tag{8}$$

Velocity of sound

$$c_2 = \sqrt{K_n(T_2)RT_2 g} \tag{9}$$

$$c_{2s} = \sqrt{K_n(T_{2s})RT_{2s}g} \tag{10}$$

Mach numbers

$$Ma_2 = V_2/c_2 \tag{11}$$

$$Ma_{2s} = V_{2s}/c_{2s} \tag{12}$$

Flow deflection at the cascade exit calculated according to Ainley

$$\Delta\alpha_2 = f\left(\frac{s_{st}}{e_{st}}, Ma_2\right) \tag{13}$$

Flow direction

$$\alpha_2 = \alpha_{B2} + \Delta\alpha_2 \tag{14}$$

Reynold number based on the passage between the blades O (for the calculation of the profile losses)

$$Re_{O2} = \frac{\beta_2 V_2 O_{st}}{\mu(T_2)} \tag{15}$$

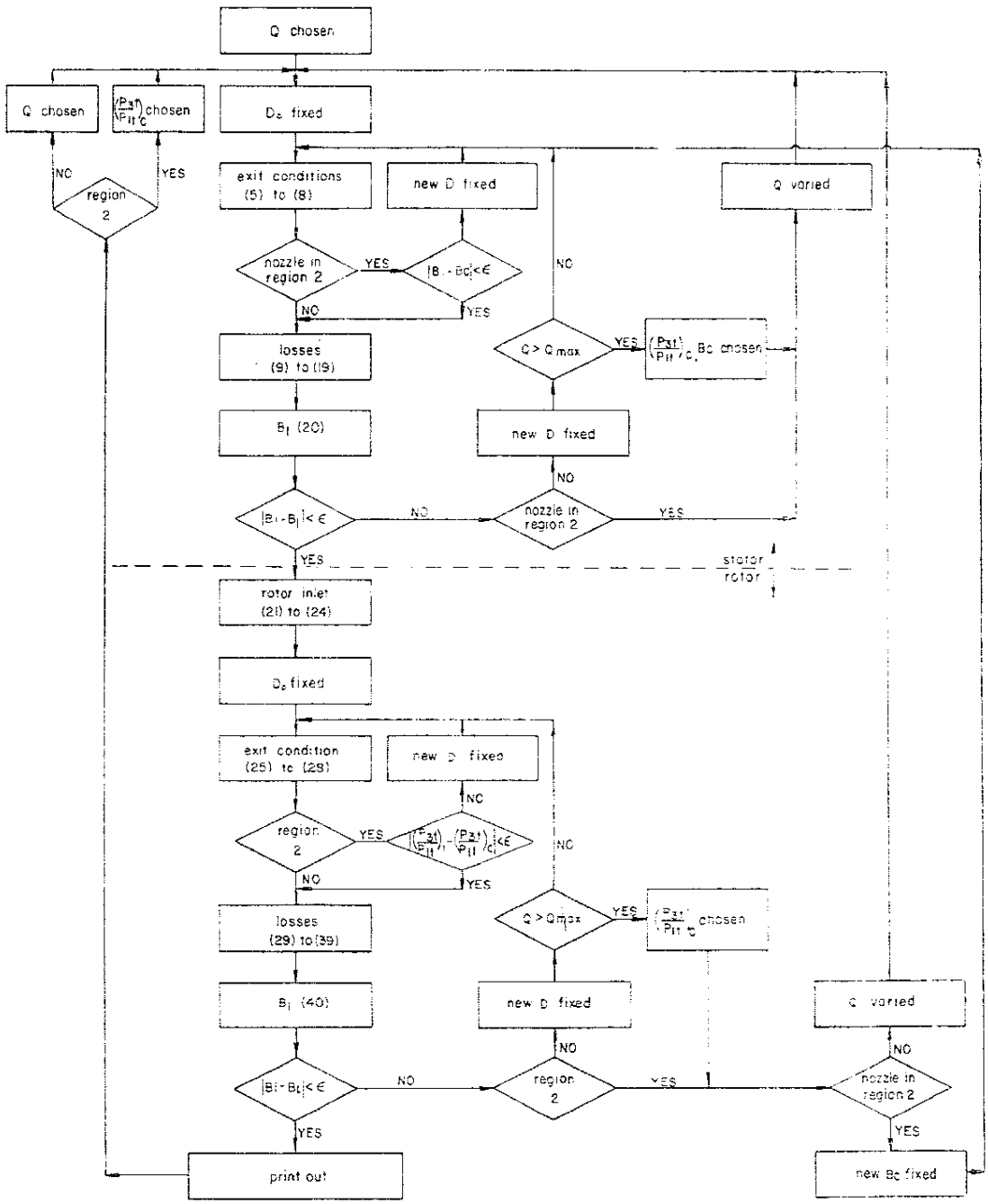

Fig. 3. Flow chart of the solution.

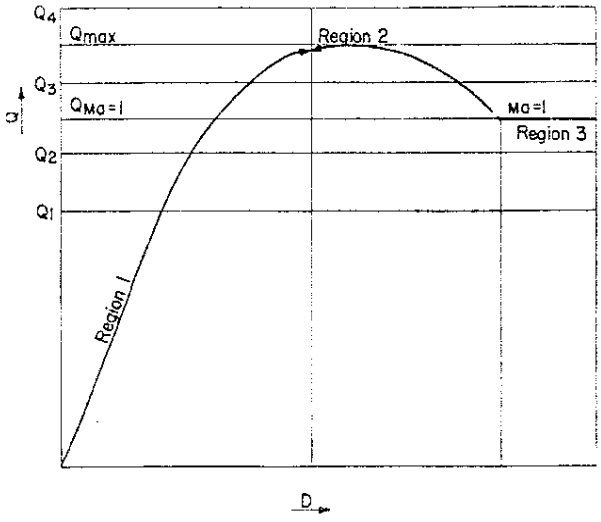

Fig. 4. The shape of the turbine characteristic.

Reynolds number based on the profile chord (for the calculation of the secondary losses)

$$Re_{C2} = \frac{\beta_2 V_2 C_{st}}{\mu(T_2)} \tag{16}$$

Profile losses according to Craig

$$X_{p\,st} = f(\alpha_{B1}, \alpha_{B2}, \alpha_1, \alpha_2, i_1, \frac{O_{st}}{s_{st}}, \frac{s_{st}}{b_{st}}, \frac{s_{st}}{e_{st}}, \frac{t_{e\,st}}{s_{st}}, Ma_{2s}, Re_{O2}) \tag{17}$$

Secondary and tip clearance losses according to Ainley

$$Y_{sc\,st} + Y_{c\,st} = f\left(\alpha_1, \alpha_2, \frac{C_{st}}{h_{e\,st}}, \frac{k_{st}}{h_{e\,st}}, \frac{t_{e\,st}}{s_{st}}, Re_{C2}\right) \tag{18}$$

Total loss factor according to Craig using Eq. (3)

$$X_{st} = X_{p\,st} + 100(T_{2s}/T_{1t})(Y_{sc\,st} + Y_{c\,st}) + X_{a\,st} \tag{19}$$

In Eq. (19) $X_{a\,st}$ the annulus loss coefficient is calculated with Craig's data. Finally the energy losses are calculated

$$\frac{J X_{st} V_2^2}{200} = \int_{T_{2s}}^{T_2} c_p(T)dT \tag{20}$$

II) Equations relevant to the rotor

Inlet conditions calculated from the inlet triangle

$$W_2 = f(V_2, u, \alpha_2) \tag{21}$$

$$i_2 = \beta_{B2} - \beta_2 \tag{22}$$

Thermodynamic conditions

$$J\frac{W_2^2}{2} = \int_{T_2}^{T_{2t\,rel}} c_p(T)dT \tag{23}$$

$$JRg \ln\frac{P_{2t\,rel}}{P_2} = \int_{T_2}^{T_{2t\,rel}} \frac{c_p(T)}{T}dT \tag{24}$$

The conditions at the rotor exit are calculated using the following equations:

Energy

$$J\frac{W_3^2}{2} = -\int_{T_{2t\,rel}}^{T_{3s}} c_p(T)dT \tag{25}$$

$$J\frac{W_{3s}^2}{2} = -\int_{T_{1t}}^{T_{2s}} c_p(T)dT \tag{25}$$

Continuity

$$G = \frac{P_3 A_3 V_3}{RT_3} \tag{27}$$

Equation of state in isentropic flow

$$JRg \ln\frac{P_3}{P_{2t\,rel}} = \int_{T_{2t\,rel}}^{T_3} \frac{c_p(T)}{T}dT \tag{28}$$

Velocity of sound

$$c_2 = \sqrt{K_p(T_2)RT_2 g} \tag{29}$$

$$c_{3s} = \sqrt{K_p(T_{3s})RT_{3s}g} \tag{30}$$

Relative Mach numbers

$$Ma_{3\,rel} = W_3/c_3 \tag{31}$$

$$Ma_{3s\,rel} = W_{3s}/c_{3s} \tag{32}$$

Flow deflection according to Ainley

$$\Delta\beta_3 = f(s_{rot}/e_{rot}, Ma_{3\,rel}) \tag{33}$$

Flow direction

$$\beta_3 = \beta_{B3} + \Delta\beta_3 \tag{34}$$

Relative Reynolds number based on passage between the blades

$$Re_{O3} = \frac{\rho_3 W_3 O_{rot}}{\mu(T_3)} \tag{35}$$

Relative Reynolds number based on blade chord

$$Re_{C3} = \frac{\rho_3 W_3 C_{rot}}{\mu(T_3)} \tag{36}$$

Profile losses according to Craig

$$X_{p\,rot} = f\left(\beta_{B2}, \beta_{B3}, \beta_2, \beta_3, i_2, \frac{O_{rot}}{s_{rot}}, \frac{s_{rot}}{b_{rot}}, \frac{s_{rot}}{e_{rot}}, \frac{t_{e\,rot}}{s_{rot}}, Ma_{3\,rel}, Re_{O2}\right) \quad (37)$$

Secondary and tip clearance losses according to Ainley

$$Y_{sc\,rot} + Y_{c\,sl} = f\left(\beta_2, \beta_3, \frac{C_{rot}}{h_{c\,rot}}, \frac{k_{rot}}{h_{e\,rot}}, \frac{t_{e\,ro\,i}}{s_{rot}}, Re_{C3}\right) \quad (38)$$

The total loss factor according to Craig using Eq. (3) is

$$X_{ro:} = X_{p\,rot} + 100\left(\frac{T_{3s}}{T_{2t\,rel}}\right)(Y_{sc\,rot} + Y_{c\,rot}) + X_{a\,rot}\frac{V_3^3}{W_3^2}. \quad (39)$$

The energy losses in the rotor are

$$\frac{JX_{ro:}W_3^2}{200} = \int_{T_{3s}}^{T_{3:}} c_p(T)dT \quad (40)$$

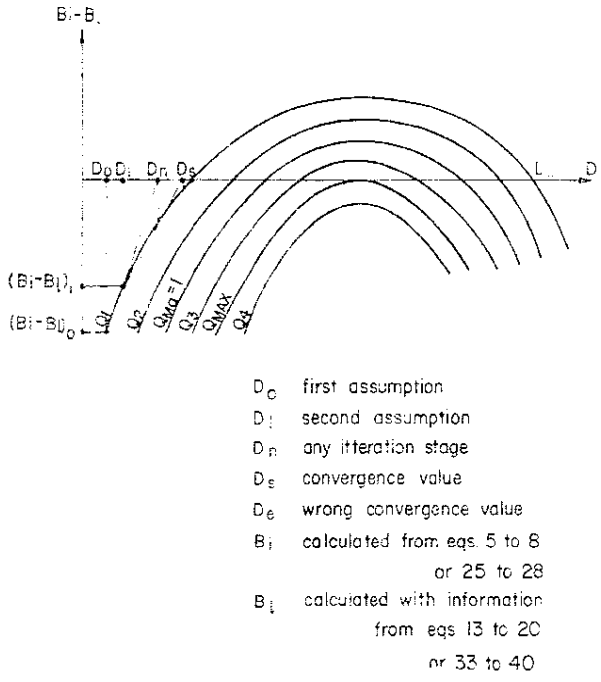

Fig. 5. Convergence of the iterative procedure in region 1.

4. THE NUMERICAL SOLUTION

As mentioned above the mathematical model of the turbine stage is solved numerically. The flow chart of the procedure is given in Fig. 3. The purpose of this paragraph is to supplement the flow chart, to elaborate some of the difficult points involved in the procedure, but not to replace Fig. 3 which includes the essentials of the solution. The iterative procedure used requires the development of an efficient convergence algorithm. This is not a simple task in this case, because the independent iteration variable used at a point depends on the location of this point on the characteristic curve. The calculation starts at low flow rates in region 1 where Q is the independent variable (see Fig. 4) The value of Q is stepwise increased until region 2 is reached, where the procedure switches over to independent variation of P_{1t}/P_{3t}. The calculation is terminated when sonic flow is detected in either nozzle or rotor, i.e. when region 3 is reached.

When Q is the independent iteration variable (region 1), the calculation is carried out in the following way, both for the nozzle or for the rotor.

a) A value is assigned to Q (see Fig. 5)

b) The value of one of the exit quantities of the cascade D_i is assumed. This quantity can be the exit pressure, the exit velocity, the exit temperature etc.

c) The remaining exit quantities are calculated using the equations of energy (5) (6), continuity (7), state (8) to (12) and the equations of the losses and related quantities (13) to (19), for the nozzle. For the rotor, Eqs. (25), (26), (27), (28) to (32) and (33) to (39) are used respectively. One of these quantities, B_i, is later used as convergence criterion.

d) Using Eq. (20) for the nozzle, the quantity B_i which was previously evaluated in step c) is recalculated and the new value, B_s compared to the previous value, B_i. For the rotor Eq. (40) is used.

e) If $B_i \neq B_s$ i.e. if convergence is not achieved, a new value B_s is assumed and the procedure repeated until the preset convergence criterion, $|B_i - B_{S_i}| < \varepsilon$, is reached. Here ε is a value as small as desired. The smaller ε is, the better the accuracy and the more iterations are required for convergence. (for $\varepsilon = 0.001$ four iterations were sufficient).

To ensure convergence, the first value assumed for D_i must be smaller than the convergence value, D_s, otherwise the solution will converge to a wrong value, D_e. The convergence procedure is based on the Newton—Raphson method. The method described above enables easy detection of unrealistic flow

rates in the nozzle or rotor ($Q > Q_{max}$) for which no solution can exist. The condition $Q > Q_{max}$ is satisfied when no convergence value can be found for D, which is an indication of an excessive flow rate.

The calculation as described above proceeds from an initial small flow rate by increasing the value of the normalised flow rate $Q = G\sqrt{T_{1t}}/P_1$ until no convergence for D can be established. This is an indication that $Q > Q_{max}$. The last value of Q for which a solution still existed, i.e. D converged, is the limit of region 1 for the nozzle or for the rotor but the exact value of Q_{max} need not be calculated. In other words, as long as convergences can be reached with Q as independent iteration variable the point of operation calculated is located in region 1. From this point onwards, P_{3t}/P_{1t} is used as an independent iteration variable. The iterative procedure here is rather complicated and involved. It can best be understood from the flow chart of Fig. 3. The entry points to this section of the solution are "yes" answers to $Q > Q_{max}$?

The entire calculation is terminated when sonic flow is reached at a point in the turbine stage.

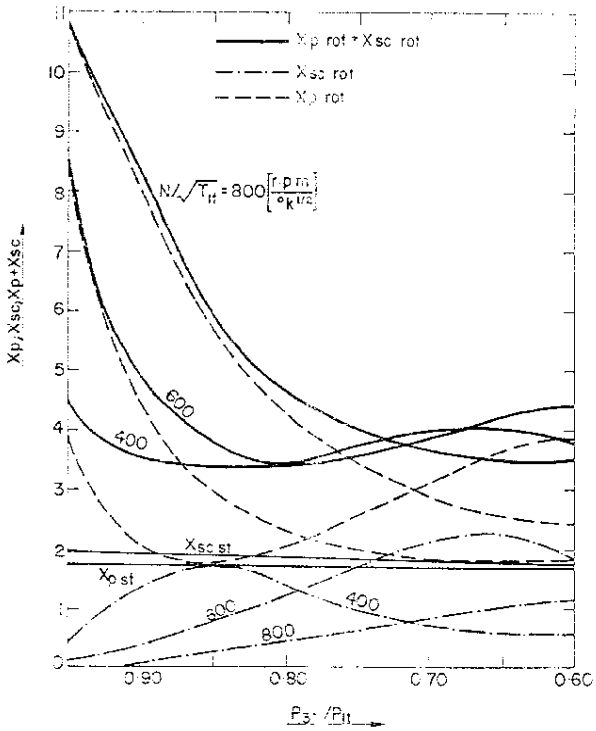

Fig. 6. Profile and secondary losses variation with the pressure ratio (stator angle $\theta = 0°$).

5. THE RESULTS

The computer model was run and tested using data of a free gas turbine of 1100 c.v. supplied by Beit Shemesh Engines Co., Beit Shemesh, Israel. Some of the results are given in Figs. 6–16. They demonstrate the ability of the mathematical model to describe a turbine stage, and analyse its performance and losses. Further, it is shown that fields of operation can be predicted for variable geometry gas turbine stages. The use of these fields of operation for the dynamic study of a turbine and the design of its control system is described by Hirsch (*Hirsch*, to be published).

The losses are basically a function of four parameters, namely: flow rate, Q, pressure ratio in the stage P_{1t}/P_{3t}, speed $N/\sqrt{T_{1t}}$ and nozzle blade angle, θ. But at given speed and θ the flow rate is a unique function of the pressure ratio so that the losses actually are a function of only three independent parameters. The losses, therefore, are presented here in two groups, (a) Figs. 6–9 where the independent parameters are speed and pressure ratio ($\theta = 0°$ being constant), (b) Figs. 10–14 where the independent parameters are θ and speed (the pressure ratio being held constant). Figure 15 shows the entire field of operation calculated and Fig. 16 gives normalized torque curves as function of the three independent parameters.

Figure 6 shows the effects of the pressure ratio and normalized speed on the loss coefficients in the nozzle and the rotor. The understanding of the nature of these loss coefficients is important as they strongly influence the performance of the turbine stage. It can be seen that substantial differences exist between the variation of the nozzle loss coefficients and the variation of the loss coefficients of the rotor. Further the fundamental difference between the variation of profile losses and the variation of secondary losses is demonstrated. In the stator both the profile loss coefficients and the secondary loss coefficients are almost constant over a wide range of speeds and pressure ratios. This is not surprising because the incidence angle of the nozzle is constant at zero and because the exit of the nozzle profile has a very small curvature. The loss coefficients of the rotor, on the other hand, are sensitive to the pressure ratio and the speed. The variation of X_p is caused by the changes in the incidence angle, i_2, on which X_p depends strongly

because of the dominant role of incidence losses. The incidence angle variation can be seen in Fig. 8 where the incidence angle is plotted against the pressure ratio for three speeds. At the design speed ($N/\sqrt{T_{1t}} = 600\ rpm/\sqrt{°K}$)$X_p$ is large at low pressure differences (high P_{3t}/P_{1t} values, small flow rates and large positive rotor incidence angles). The value of X_p reduces with increasing pressure difference and flow rate as the incidence angle reduces (Fig. 8). The smallest X_p value is reached for $Q = 142(m^2\sqrt{°K}/sec)$ and $P_{3t}/P_{1t} = 0.6$, this is the design point as also confirmed by engine tests. The variation of X_p with the pressure ratio in the vicinity of the design point ($P_{3t}/P_{1t} = 0.6$) at all speeds is small, because in this region the flow in the rotor approaches sonic velocity reducing the possible variation of the flow rate. The effect of speeds on X_p is large at small pressure differences where the flow rate and through flow velocities are small. This sensitivity of X_p is due to the large variation of the incidence angle as is evident from Fig. 8.

The variation of the secondary losses in the rotor is entirely different. These losses are caused mainly by the pressure gradients in the flow field. These are an increasing function of the flow deflection and energy conversion in the cascade (affecting the pressure difference between suction side and pressure side of the profile). The energy conversion in the rotor is most effective when profile losses are small i.e. near the design point, and therefore the values of X_{sc} is large when X_p is small.

Figure 7 describes the variation of the main profile loss coefficient components, X_{PB}, N_{Pi}, N_{PT} and N_{PR} with the pressure ratio. These are related to X_p in the following equation of Craig.

$$X_p = X_{PB}N_{PR}N_{Pi}N_{PT} + (X_p)_{tr} + (X_p)_{s/e} + (X_p)_M. \tag{41}$$

Figure 7a shows the variations of the basic profile loss factor; these variations are caused mainly by loading. Indirectly, however, the basic loss factor is influenced by the incidence angle and therefore it reaches its minimum at low incidence angles (see Fig. 8) near the design point. The variation of the basic loss factor over the entire range examined is about 25%. Figure 7b gives the incidence loss factor

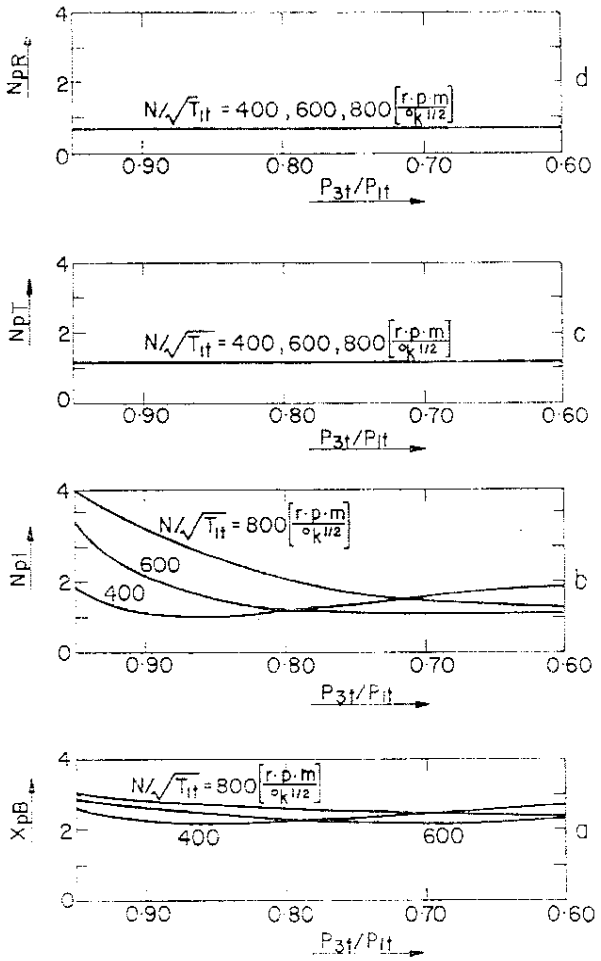

Fig. 7. Correction factors variation with the pressure ratio (stator angle $\theta = 0°$)

which is the most dominant influence factor on the efficiency and on the performance variation as function of the point of operation. Its variation over the range investigated is about 35%. The coupling of this loss factor with the incidence angle is evident from Fig. 8. The trailing edge loss coefficient is constant (Fig. 7c) because its main parameter of influence is the blade geometry which is fixed. Figure 7d shows the Reynolds number influence factor which is also almost constant because the dependence of the profile loss on *Re* is weak and because the variation of *Re* over the range of operation investigated is not large enough to cause a meaningfull effect (see Fig. 9).

Let us now analyse the effect of the nozzle blade angle, θ, on the turbine performance when the pressure

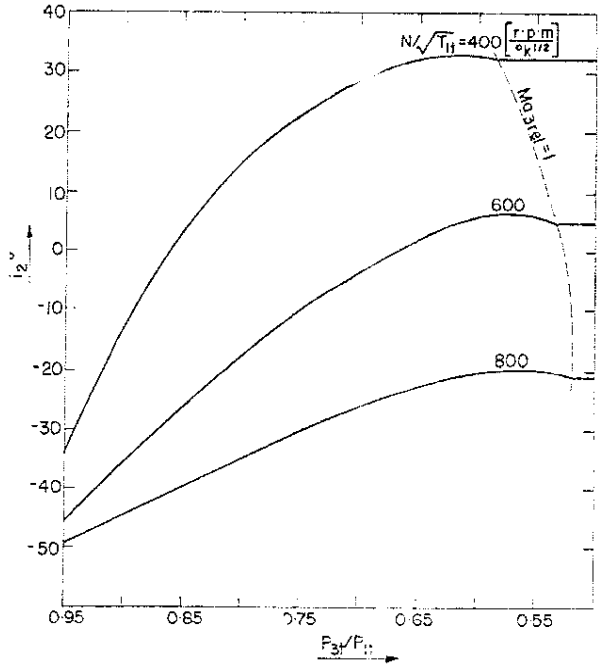

Fig. 8. Variation of the rotor incidence angle with the pressure ratio (stator angle $\theta = 0°$).

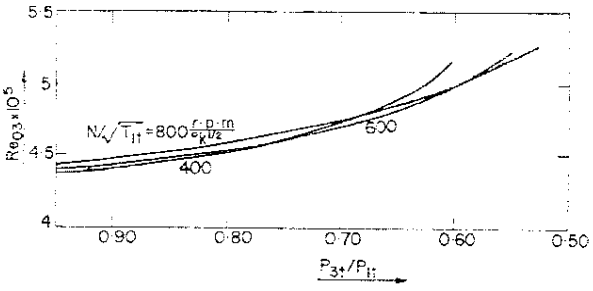

Fig. 9. Reynolds number variation over the pressure ratio range investigated (stator angle $\theta = 0°$).

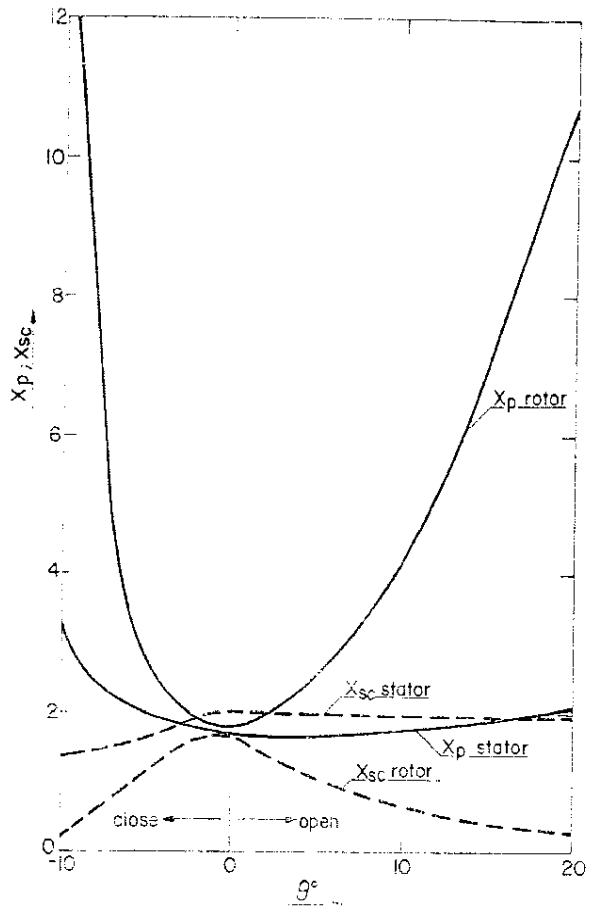

Fig. 10. Profile and secondary losses variation with the stator vane position (Pressure ratio $P_{3t}/P_{1t} = 0.6$)

ratio is kept constant. A variation of θ from the design point at which $\theta = 0°$ affects mainly the rotor losses as can be seen in Fig. 10. Here a strong influence on X_p is observed, while the secondary losses are less sensitive. The losses in the nozzle $(X_p + X_{sc})_{st}$ are much less sensitive to θ variations because the increase in X_p is partially compensated by a decreasing X_{sc}. Nozzle losses are less sensitive to θ variation than rotor losses because in the nozzle no energy is converted as is the case in the rotor. This result confirms Rahnke's observations.

The partial losses are described in Fig. 11 where, like in Fig. 7 and because of the same reasons, trailing edge losses and Reynolds effects are almost constant. The not significant Re variation is shown in Fig. 13. Incidence losses again are most dominant and play a major role because of the large incidence angle variations, as shown in Fig. 12. These results again confirm Rahnke's report.

Combination of all the partial losses discussed so far result in the overall stage efficiency shown in Fig. 14. As expected the best efficiency is reached at the design point ($\theta = 0°$). When extrapolating the curves to large θ values the efficiency becomes negative, i.e. the turbine works as a compressor acting as a braking device when installed in a vehicle.

Figure 15 gives the predicted field of operation of the turbine stage. To avoid confusion the lines of constant efficiency (given in Fig. 14) are omitted. Each

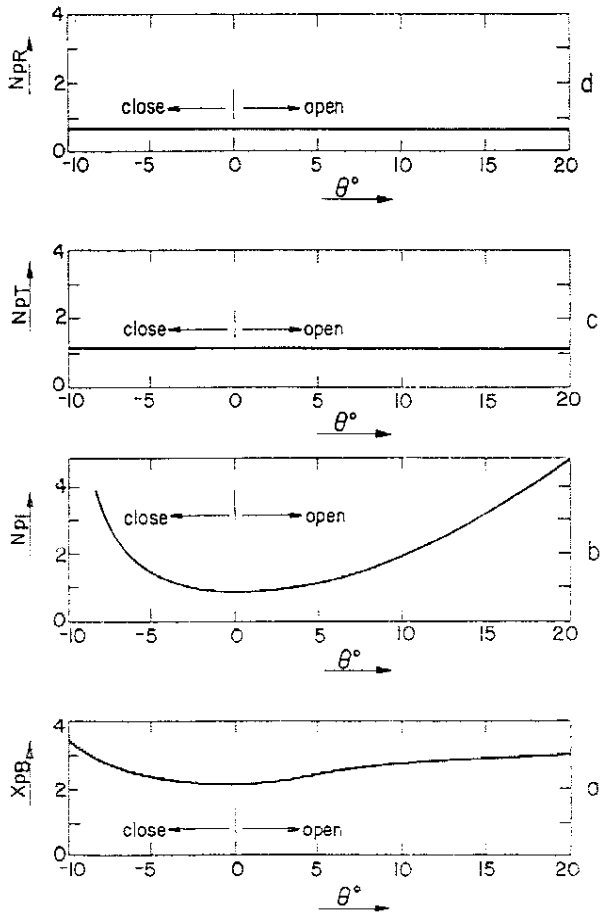

Fig. 11. Correction factors variation with the stator vane position (pressure ratio $P_{3t}/P_{1t}=0.6$).

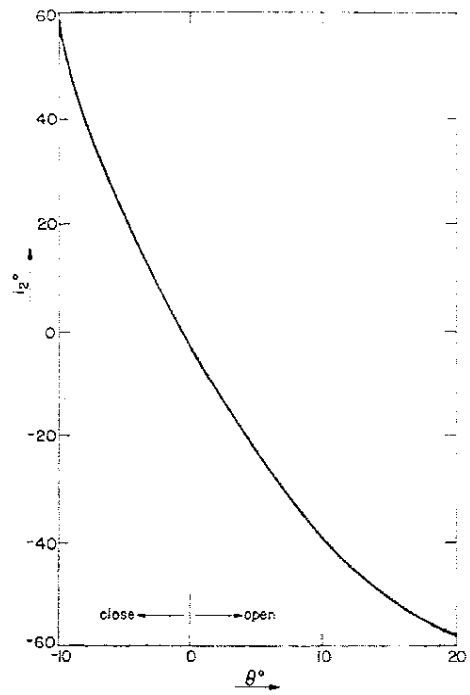

Fig. 12. Variation of the rotor incidence angle with the stator vane position (pressure ratio $P_{3t}/P_{1t}=0.6$).

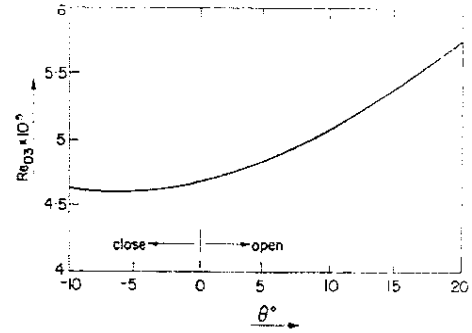

Fig. 13. Reynolds number variation with the stator vane position (pressure ratio $P_{3t}/P_{1t}=0.6$).

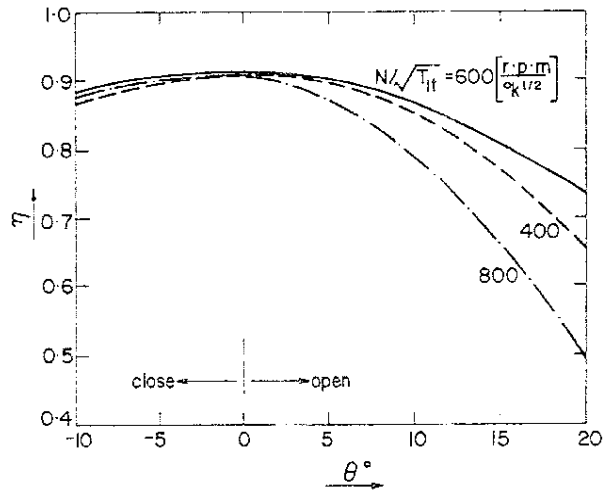

Fig. 14. Total efficency of the turbine stage as function of the stator vane position (pressure ratio $P_{3t}/P_{1t}=0.6$).

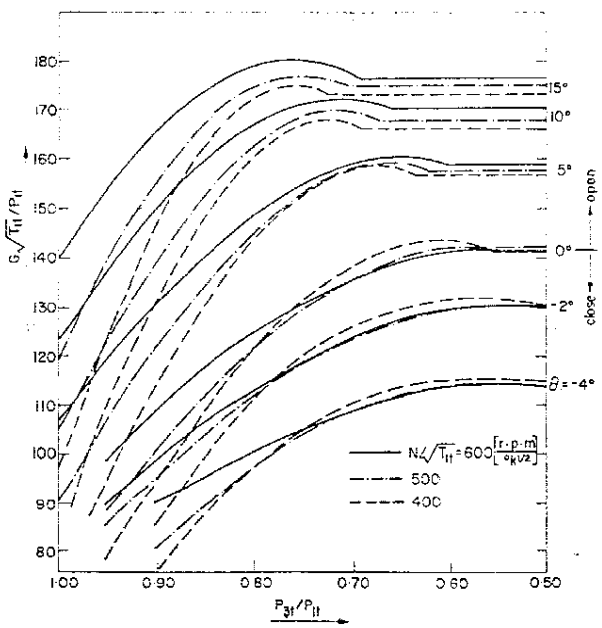

Fig. 15. Field of operation of the turbine stage.

group of curves, related to a given θ value, describes the normalized flow rate vs. stage pressure ratio, with the normalized speed as parameter. The flow rate increases with increased pressure difference over the stage, it reaches a maximum value and drops to the chocking point. From there onwards the flow rate is constant. The more the nozzle blades are opened, the earlier choking occurs because with opened vanes at a given pressure ratio the velocities in the stage are increased, and this means that the degree of reaction is increased (or that the rotor exit velocities are larger). This causes earlier choking.

For every group of curves the difference between the maximum flow rate and the choking flow rate is increased with the nozzle blade opening. This is caused by the combined effect of the increase of the losses and the increase of the velocities when the nozzle blades are opened. When the nozzle blades are closed to negative θ values only the losses increase but the velocities decrease. At an open nozzle blades position, when both the loss and the velocity levels are high, an increase in the pressure difference (causing an additional increase of the already high velocities) is coupled with a sharp increase of the losses even when the loss factors grow only slightly. This effective increase of the losses causes the marked flow rate reduction towards the choking point. With closed nozzle blades the flow rates and the velocity level are low, so that the flow rate reduction towards the choking point is less pronounced.

The effect of the opening of the nozzle blades at constant speed and pressure ratio on the flow rate is obvious. In the region near the design point the increase in flow rate with θ is not linear. Extrapolating in the direction of opened nozzle blades it can be seen that the flow rate reaches a maximum at around $\theta = 25°-30°$, as can be expected. This maximum is a result of the flow passage area variation with increasing θ and the loss increase when the nozzle blades are opened (*Rahnke*, 1969).

Normalized torque curves of the turbine stage are given in Fig. 16. It must be pointed out here that the torque presented is not the torque of a complete gas turbine (which is the result of a combined performance of compressor stages, combustion chamber and turbine stages) but rather the torque of an isolated stage. At constant pressure ratio and nozzle blade position the torque drops with increased speed because with all other parameters held constant the torque is inversly proportional to the speed.

Finally, Figs. 17 and 18 compare results calculated

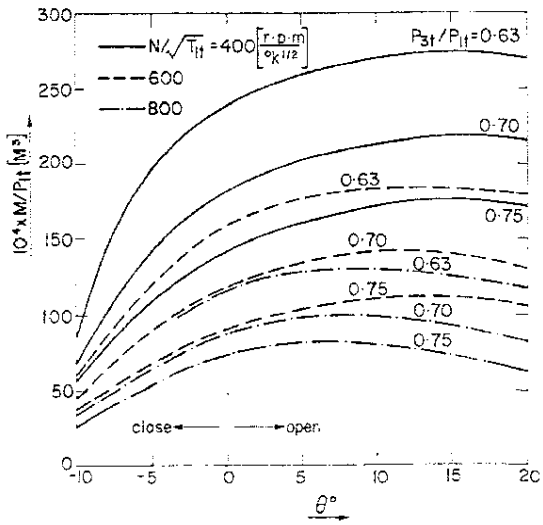

Fig. 16. Torque curves of the turbine stage.

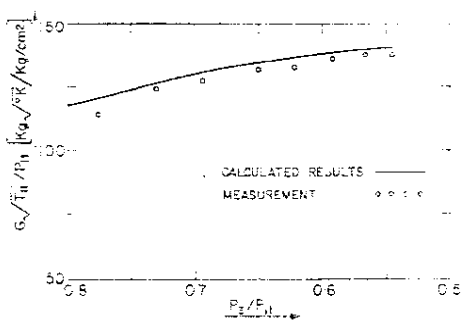

Fig. 17. Comparison between a calculated and a measured operation curve for $\theta=0°$ ($N/\sqrt{T_{1t}}$ is not constant on the curve).

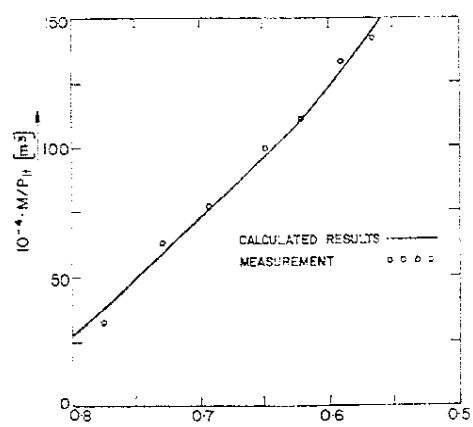

Fig. 18. Comparison between a calculated and a measured operation curve for $\theta=0°$ (N/T_{1t} is not constant on the curve). Torque was measured at the exit shaft of a 6:1 reduction gear box, calculations were accordingly scaled.

using the present method with experimental results. The experiments were carried out on the 1100 c.v. gas turbine at one of the test cells of the Beit Shemesh Engines Co. During the experiments $N/\sqrt{T_{1t}}$ could not be kept at a constant value, it varied monotonously from $N/\sqrt{T_{1t}} = 675$ rpm/°K$^{\frac{1}{2}}$ at $P_3/P_{1t} = 0.848$ to 604 rpm/°K$^{\frac{1}{2}}$ at a pressure ratio of 0.545. The agreement between the calculated curves and measured points is good enough to have some confidence in the method. The largest errors occur at large pressure ratios (small pressure differences over the turbine), well away from the design point where the torque is very low. In the region of operation the errors are about 4% for the normalized torque M/P_{1t} and 2.5% for the normalized flow rate $G\sqrt{T_{1t}}/P_{1t}$. However, more experiments are needed; these are planned for the future.

AKNOWLEDGEMENTS

The authors wish to mention the valuable contribution of Mr. J. Sinai, Chief Engineer of Beit Shemesh Engines Co., Beit Shemesh, Israel, and of his firm to this work. Further they would like to express their appreciation to Mr. A. Halfon of the Technion for his computer work.

REFERENCES

AINLEY, D. G. AND G. C. R. MATHIESON, 1957. A method of performance estimation for axial-flow turbines, Ministry of Supply — Aeronautical Research Council Report and Memoranda.

CRAIG, H. R. M. AND H. J. A. COX, 1970–71, Performance estimation of axial flow turbines, The Institution of Mechanical Engineers, *Thermodynamics and Fluid Mechanics*, Proceedings, Volume 185,32/71.

DUNHAM, J. AND P. M. CAME, 1970. Improvement to the Ainley — Matheison method of turbine performance prediction, ASME Publication Paper No. 70-GT-2.

HAWTHORN, W. R., 1964. *Aerodynamics of Turbines and Compressors*, Oxford University Press, London.

HIRCSH, M., Y. DAYAN AND D. ADLER, Dynamic and control of a gas turbine engine with a variable geometry free power turbine, to be published.

J. H. HORLOCK, 1966. *Axial Flow Turbines*, London, Butterworths.

RAHNKE, C. J., 1969. The variable-geometry power turbine. S. A. E. Paper 690031: International Automotive Engineering Congress, Detroit, Mich., January 13–17, 1969.